Refractive-index sensitivities of hybrid surface-plasmon resonances for a core-shell circular silver nanotube sensor

Elena A. Velichko* and Alexander I. Nosich

Laboratory of Micro and Nano Optics, Institute of Radio-Physics and Electronics NASU, Kharkiv 61085, Ukraine
**Corresponding author: elena.vel80@gmail.com*

Received September 2, 2013; revised October 22, 2013; accepted October 22, 2013;
posted October 25, 2013 (Doc. ID 196135); published November 21, 2013

We study the scattering and absorption of an H-polarized plane electromagnetic wave by a circular silver nanotube in the visible range of wavelengths using the separation of variables. The computed spectra of the extinction cross section display several hybrid localized surface-plasmon resonances of the dipole and multipole type. Analytical equations are derived for their resonance wavelengths. Bulk refractive-index sensitivities of nanotube-based sensors are determined, showing higher values for multipole resonances.

OCIS codes: (290.0290) Scattering; (240.6680) Surface plasmons; (280.4788) Optical sensing and sensors.
http://dx.doi.org/10.1364/OL.38.004978

In today's nanotechnologies, finite-length gold and silver nanowires are widely used as building blocks of biosensors thanks to the localized surface plasmon (LSP) resonances. In dense "bed-of-pins" sensor configurations [1,2], only transversal LSP resonances are excited efficiently. Their wavelengths are determined by the wire cross section and the refractive index of outer medium [3]. The simplest case is a circular wire. However, for a silver wire in free space, the transversal LSP resonance is located at ≈350 to 370 nm where absorption is large. More attractive for applications are nanotubes whose LSP resonances can be tuned to larger wavelengths by the variation in tube thickness [4–7].

It is known that LSP modes on thin-wall metal nanoshells display hybridization (see [8–10]). This is caused by the *surface* nature of plasmon oscillations: a tube has two boundaries, the inner one and the outer one, each of which supports its own LSP mode of a void and a circular wire, respectively. Still the details of hybridization of the higher-order LSP modes remain less studied than of the fundamental dipole plasmons. Our aim is to clarify this effect and estimate its potential for the sensing applications.

To analyze the nanotube resonances in detail, we consider an H-polarized electromagnetic plane wave normally incident on an infinite circular silver tube of the inner radius a and thickness h [see inset in Fig. 1(b)]. Using the classical separation of variables in the tube cross section [11], the scattered field is found analytically in the form of infinite Fourier series with known coefficients.

In Fig. 1, we present the visible-range spectra of the total scattering cross section (TSCS) and absorption cross section (ACS) of the nanotube with $a = 50$ nm and several values of thickness h. Here the complex-valued dielectric function of silver has been taken from [12], and the tube inner material and the host medium are free space.

As one can see, if the tube thickness approaches 80 nm, there is only one well visible LSP-resonance peak at nearly the same wavelength (≈370 nm) as for a solid circular nanowire. In contrast, thinner tubes show several resonances redsifted and blueshifted from the circular-wire LSP-resonance wavelength. Note that the absorption can serve as a finer instrument of detecting the multipole LSP resonances than the scattering, especially in the violet part of the spectrum.

For a subwavelength-radius tube, characteristic equations for the natural mode wavelengths can be derived in analytical form using the small-argument asymptotics of cylindrical functions in denominators of the Rayleigh-series solution (see [5,11]),

$$\left(\frac{a}{a+h}\right)^{2m} + \frac{(\varepsilon_{\text{out}} + \varepsilon_{Ag})(\varepsilon_{Ag} + \varepsilon_{\text{in}})}{(\varepsilon_{\text{out}} - \varepsilon_{Ag})(\varepsilon_{Ag} - \varepsilon_{\text{in}})} + O[k^2(a+h)^2\varepsilon] = 0, \tag{1}$$

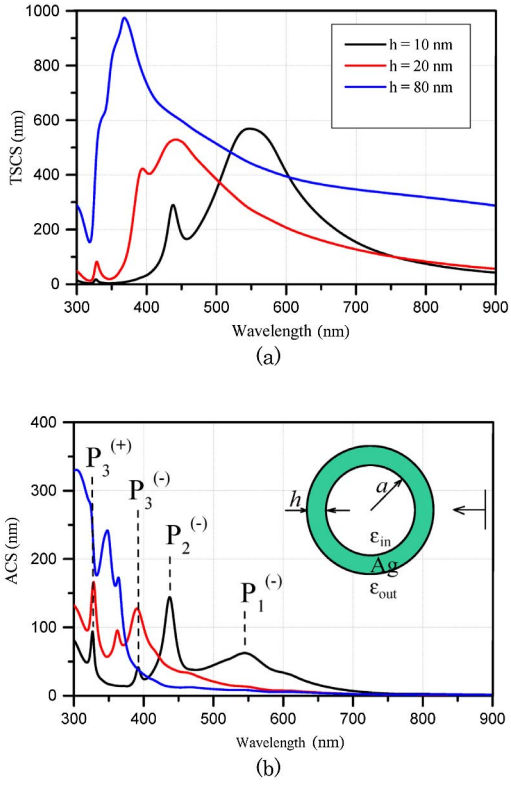

Fig. 1. (a) TSCSs and (b) ACSs versus the wavelength, for an Ag tube of the inner radius $a = 50$ nm in free space. For the thickness h see the inset. Inset shows cross section of the tube.

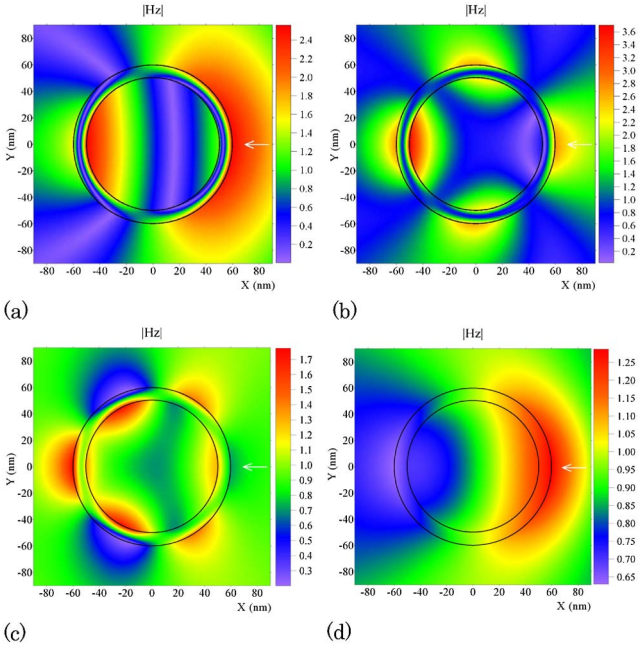

Fig. 2. In-resonance near-zone magnetic field patterns for an Ag tube with $a = 50$ nm and $h = 10$ nm located in free space, at the wavelengths of (a) $\lambda = 545$, (b) 437, (c) 392, and (d) 327 nm.

where $m = 1, 2, \ldots$ and $\varepsilon_{\text{out}}(\varepsilon_{\text{in}})$ is the dielectric permittivity of the host medium (inner filling).

If the inner and outer domain refractive indices are the same ($\varepsilon_{\text{in}} = \varepsilon_{\text{out}} = \varepsilon$), then approximate wavelengths of the LSP resonances of the azimuthal order m are found to satisfy

$$\varepsilon_{Ag}(\lambda_{Pm}^{(\pm)}) \approx -\varepsilon \pm 2\varepsilon[(1+h/a)^m \pm 1]^{-1}, \quad m = 1, 2, \ldots \quad (2)$$

For each m Eq. (2) has two roots $\lambda_{Pm}^{(\pm)}$ corresponding to the choice of the sign ($\pm$); the wavelength of each is specific for every metal and depends on the parameters ε and h/a. One of them is seen at a larger λ than for a solid silver circular nanowire and the other at a smaller λ. Equation (2) enables us to determine that three resonances marked in Fig. 1 on the red side of the solid-wire resonance wavelength of 350 nm are caused by the dipole, quadrupole, and hexapole LSP modes ($m = 1, 2, 3$) of the sign (–) in Eq. (2).

In-resonance magnetic near-field patterns are dominated by the natural-mode contributions, see the maps of $|H_z|$ in Figs. 2(a)–2(c). Each of them demonstrates $2m$ bright spots sticking to the inner and outer walls and zero field near to median circle.

Note that the quadrupole LSP has larger Q factor than the dipole one. This is apparently because of a larger

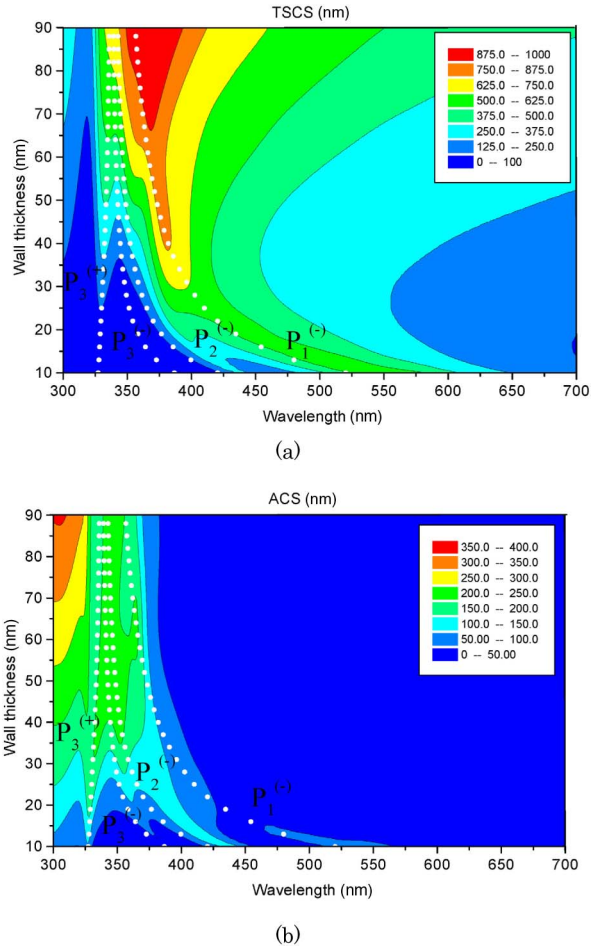

Fig. 3. Reliefs of (a) TSCS and (b) ACS as a function of the wavelength and the nanotube thickness for an Ag tube of the inner radius $a = 50$ nm.

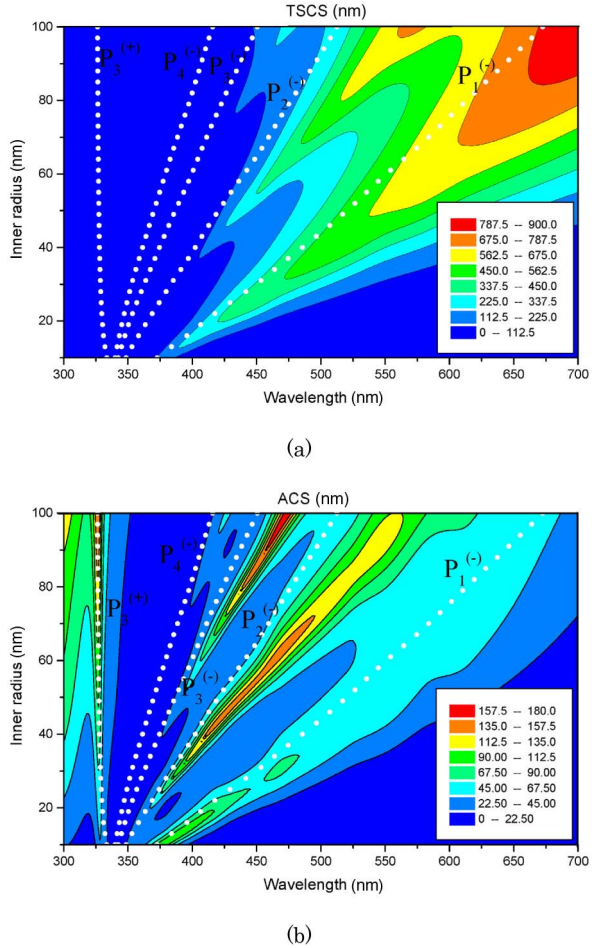

Fig. 4. Reliefs of (a) TSCS and (b) ACS as a function of the wavelength and the nanotube inner radius for an Ag tube of the wall thickness $h = 10$ nm.

number of the electric-field minima around the tube (at the locations of the magnetic-field maxima) that damps the absorption.

For comparison, Fig. 2(d) presents near field at 327 nm corresponding to the most blueshifted peak in Fig. 1. This peak is the combined contribution of three hybrid LSP modes corresponding to the sign (+) in Eq. (2) and $m = 1, 2, 3$, with the dipole one dominating.

Closer study reveals that each of the above-mentioned nanotube modes at $\lambda_{Pm}^{(\pm)}$ is a hybrid mode or supermode (in the same sense as for microcavities [13]). They are built on optically coupled in-phase or antiphase LSP modes of the index m of the outer boundary and the inner (void) boundary. Note that their quality factors are different, $Q_m^{(+)} \gg Q_m^{(-)}$.

To illustrate the optical response of a silver nanotube in a more complete manner, we present, in Fig. 3, the reliefs of TSCS and ACS versus two variables, λ and the wall thickness, for a silver nanotube with the fixed inner radius of 50 nm.

Here, the minimum thickness is taken as 10 nm to justify the neglect of the nonlocal effects in silver. According to [6,14], such effects become significant in the metal particles smaller than 3–5 nm.

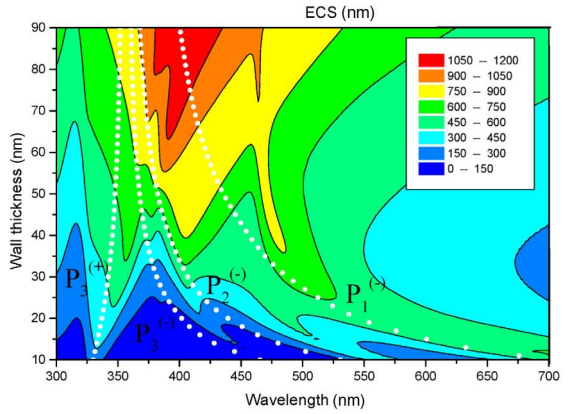

(a)

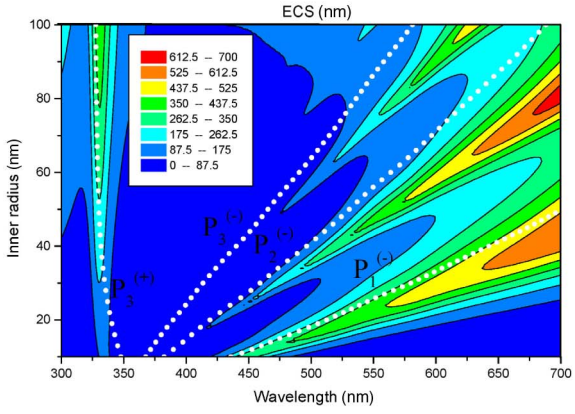

(b)

Fig. 5. Reliefs of ECS (a) as a function of the wavelength and the wall thickness, for a nanotube with $a = 50$ nm, and (b) as a function of the wavelength and the inner radius, for a nanotube with $h = 10$ nm. Silver nanotube has a glass core and is immersed in water, as explained in text.

As one can see, the reliefs of TSCS and ACS show bright "ridges" as contributions of the higher-order LSP modes $P_m^{(-)}$ with $m = 2, 3$ in addition to the principal LSP mode $P_1^{(-)}$. The contributions of all blueshifted hybrid LSP modes $P_m^{(+)}$ merge together into one high-Q ridge. The white dotted lines show the values of resonance λ that satisfy quasi-static equation (2); they agree within 10% margin with the full-wave data if $a + h \leq 50$ nm.

In Fig. 4, we show similar reliefs of TSCS and ACS computed for the silver nanotube with the wall thickness of 10 nm and varying inner radius. If $a > 80$ nm, then even the octupole LSP becomes visible on the ACS relief and three plasmons $P_{1,2,3}^{(-)}$ are present on both the ACS and

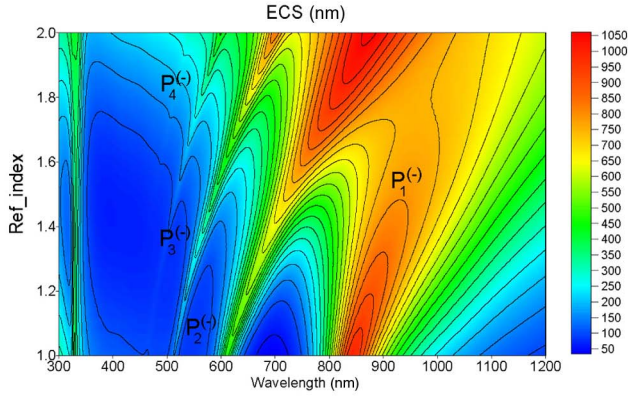

(a)

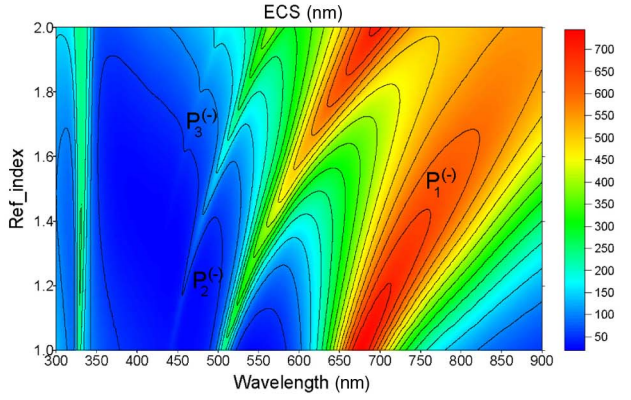

(b)

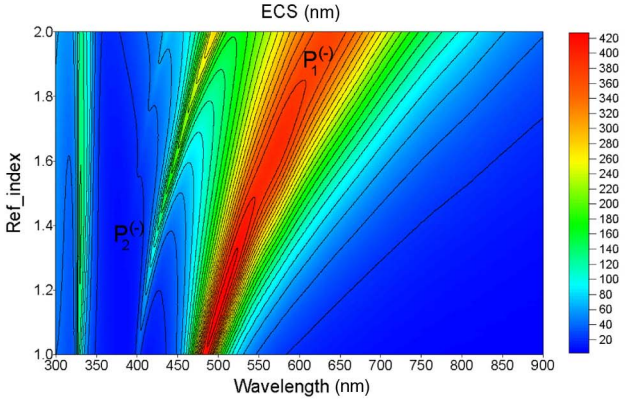

(c)

Fig. 6. Reliefs of ECS as a function of λ and the outer medium refractive index, for a nanotube having the wall thickness $h = 10$ nm and the inner radius (a) $a = 80$, (b) 50, and (c) 20 nm.

Table 1. Sensitivities of Hybrid LSPs

a, LSP Type	S, nm/RIU	W, nm at R.I. = 1.4	FOM
80 nm, $P_1^{(-)}$	188	330	0.6
$P_2^{(-)}$	265	100	2.7
$P_3^{(-)}$	185	33	5.6
$P_4^{(-)}$	140	30	4.7
50 nm, $P_1^{(-)}$	225	203	1.1
$P_2^{(-)}$	190	50	3.8
$P_3^{(-)}$	125	25	5
20 nm, $P_1^{(-)}$	157	75	2.1
$P_2^{(-)}$	94	13	7.2

TSCS reliefs for all values of the inner radius. The quasi-static approximations to $\lambda_{Pm}^{(\mp)}$ are shown by white dots.

Having basic properties of a silver nanotube in free space clarified, we can better understand the optical response of a core-shell nanowire—silver nanotube filled with material ε_{in} and placed into medium ε_{out}.

In this case, a more general equation than Eq. (2) is

$$\varepsilon_{Ag}(\lambda_{Pm}^{(\pm)}) \approx -\frac{(\varepsilon_{\text{in}}+\varepsilon_{\text{out}})}{2}\xi_m \pm \left[\frac{(\varepsilon_{\text{in}}+\varepsilon_{\text{out}})^2}{4}\xi_m^2 - \varepsilon_{\text{in}}\varepsilon_{\text{out}}\right]^{1/2}, \tag{3}$$

where $\xi_m = (1+\gamma^{2m})/(1-\gamma^{2m})$, $\gamma = a/(a+h)$, $m = 1, 2, \ldots$

Keeping also in mind that, in the measurements, it is difficult to separate the scattered power from the absorbed power, we present the reliefs of the extinction cross section (ECS), which is the sum of TSCS and ACS, see Fig. 5 [white dots satisfy Eq. (3)]. As realistic values of material parameters, in these computations we took $\varepsilon_{\text{in}} = 2.25$ for a glass core and $\varepsilon_{\text{out}} = 1.96$ for a water-like host medium [2,6].

Finally, we assess the two most important characteristics of a nanosensor: the bulk sensitivity S of the refractive index $\sqrt{\varepsilon_{\text{out}}}$ and the figure-of-merit (FOM) F, which is S divided by the full width of resonance at the half-peak level, W (see [1,2]).

In Fig. 6, we present the reliefs of ECS for glass-core sensors immersed into a medium with refractive index varying from 1 to 2. Multimode response caused by the higher-order hybrid antiphase LSP modes is excellently visible. In the most typical scenario, we can assume that the analyte refractive index is close to 1.4, which corresponds to a water solution of proteins (see [2]). The corresponding values of S, W, and FOM extracted from these reliefs are shown in Table 1.

As visible, the best bulk refractive-index sensitivity of 265 is associated with the quadrupole LSP resonance $P_2^{(-)}$ on the silver nanotube with an 80 nm glass core, and the best FOM of 7.2 with the same LSP mode on a 20 nm core. The multipole sensors are generally preferable to the dipole-based ones. Note that the sensitivity can be raised if the sensed material additionally fills the core of the nanotube [2].

This work has been supported by the National Academy of Sciences of Ukraine via the State Target Program "Nanotechnologies and Nanomaterials."

References

1. J. McPhillips, A. Murphy, M. P. Jonsson, W. R. Hendren, R. Atkinson, F. Hook, A. V. Zayats, and R. J. Pollard, ACS Nano **4**, 2210 (2010).
2. A. Murphy, Y. Sonnefraud, A. V. Krasavin, P. Ginzburg, F. Morgan, J. McPhillips, G. Wurtz, S. A. Maier, A. V. Zayats, and R. Pollard, Appl. Phys. Lett. **102**, 103103 (2013).
3. O. J. F. Martin, in *Optical Nanotechnologies*, *Topics in Applied Physics*, J. Tominaga and D. P. Tsai, eds. (Springer, 2003), pp. 183–210.
4. J. Zhu, Mater. Sci. Eng. **454–455**, 685 (2007).
5. H.-Y. She, L.-W. Li, O. J. F. Martin, and J. R. Mosig, Opt. Express **16**, 1007 (2008).
6. J. M. McMahon, S. K. Gray, and G. C. Schatz, J. Phys. Chem. **114**, 15903 (2010).
7. H. Xu, H. Li, Z. Liu, S. Xie, X. Zhou, and J. Wu, Solid State Commun. **151**, 759 (2011).
8. C. Radloff and N. J. Halas, Nano Lett. **4**, 1323 (2004).
9. Y. Wu and P. Nordlander, J. Chem. Phys. **125**, 124708 (2006).
10. F. Hao, Y. Sonnefraud, P. V. Dorpe, S. A. Maier, N. J. Halas, and P. Nordlander, Nano Lett. **8**, 3983 (2008).
11. Lord Rayleigh, Philos. Mag. **12**(73), 81 (1881).
12. P. B. Johnson and R. W. Christy, Phys. Rev. B **6**, 4370 (1972).
13. E. I. Smotrova, T. M. Benson, P. Sewell, J. Ctyroky, and A. I. Nosich, J. Opt. Soc. Am. A **25**, 2884 (2008).
14. G. Toscano, S. Raza, A.-P. Jauho, N. A. Mortensen, and M. Wubs, Opt. Express **20**, 4176 (2012).